Device-free Human Tracking Exploiting Phase Disturbances and Particle Filters

Anastasios Tzitzis, Aristidis Raptopoulos Chatzistefanou, Spyros Megalou,
Stavroula Siachalou, Traianos Yioultsis, Antonis G. Dimitriou
School of Electrical and Computer Engineering, Aristotle University of Thessaloniki, Thessaloniki, Greece
antodimi@ece.auth.gr

***Abstract*—This work presents a phase-based device-free localization (DFL) scheme for tracking the movement of a human target by employing a network of anchor RFID tags inside the search space. The proposed method measures the phase disturbances of the backscattered field induced by a target roaming in the propagation environment and detects whether an antenna-to-tag link is obscured or not. This binary information is fused by a geometrical model that realises the target as a cylinder, thanks to which the position of the target can be identified even by a single reader-antenna. A particle filter algorithm (PF) keeps track of the target's movement over time, smoothing otherwise abrupt maneuvers. Experimental results with a single antenna report a median absolute localization error in the order of 20cm which decreases to 15cm when more antennas are employed. The real-time capability of the method is also verified.**

***Index Terms*—RFID, device-free localization, human tracking**

I. Introduction

Localization and tracking is a key feature for numerous applications. As such, it has received great attention and has been treated in depth in prior art. Device-free localization (DFL) methods have the advantage of not requiring any operational device on the target, but suffer from the inability to identify the target. On the other hand, in contrast to device-based methods, they are not constrained by the demand for continuous operation of the target's device. DFL methods employ a network of RF sensors around the monitored space. The presence or movement of a human target inside the propagation environment is expected to induce disturbances of the measured radio patterns. The target can be thus localized on account of such observed changes.

In the majority of DFL methods, disturbances of the received signal strength (RSS) measured from distributed RF sensors are used to localize the target. Some representative techniques are:

- Propagation model-based [1] - [3]: These techniques refer to the modeling of radio signal phenomena such as scattering, diffraction, fading, etc, with a mathematical model, capable of mapping online measurements to target locations. For this purpose, data from extensive experiments should be collected in order to define an accurate model. However, this can be a quite challenging task, while the model is environment-dependent and can not be used globally.
- Fingerprinting [4], [5]: Instead of using a mathematical model, fingerprinting-based methods necessitate the construction of a reference radio map by collecting data with a target placed at several predetermined positions. The target is localized by matching the collected measurements to the reference radio map. Gathering reference measurements is a time-consuming process and should be repeated in case of repositioning a sensor or an object.
- Training-based [6] - [9]: Similarly, training-based methods introduce the prerequisite of having training set of measurements for all target positions. Such set is used to feed and train a neural network. The latter incorporates new measurements to output the target's position.
- Radio Tomographic Imaging (RTI) [10] - [12]: Inspired by the medical tomography, the search space is surrounded by transmitters and receivers to construct an image that releases the location of the target in it. RTI methods use a linear model to compute the attenuation field over the space. Although promising, multiple antennas are required to surround the space of interest which is not always applicable.
- Other: [13], [14] localize a human target by utilizing information about the angle of arrival and interference effect, respectively.

In this paper, a low-cost DFL module is presented, which employs a set of passive RFID tags to track a moving human target. A single or more closely spaced antennas are employed at one side of the monitored area to measure the backscattered signal of each RFID tag. The fluctuations of phase measurements are utilized to identify whether an antenna-to-tag link is interfered by a human occurrence. Phase measurements are stored in a two-state model indicating whether the link is obstructed or not. This binary-state information is then fused by a geometrical model, according to which the target holds a cylindrical volume. Electromagnetically modeling the human body as a conducting cylinder was shown experimentally in [15]. This model is fused with a target transition model by a bayesian particle filter algorithm to update the positions of the

This research has been co-financed by the European Union and Greek national funds through the Operational Program Competitiveness, Entrepreneurship and Innovation, under the call RESEARCH – CREATE – INNOVATE (project code:T2EDK-02000).

978-1-6654-1046-5/22/$31.00 ©2022 IEEE

2022 IEEE International Conference on RFID (RFID) | 978-1-6654-1046-5/22/$31.00 ©2022 IEEE | DOI: 10.1109/RFID54732.2022.9795987

Authorized licensed use limited to: Aristotle University of Thessaloniki. Downloaded on September 26,2022 at 08:46:46 UTC from IEEE Xplore. Restrictions apply.

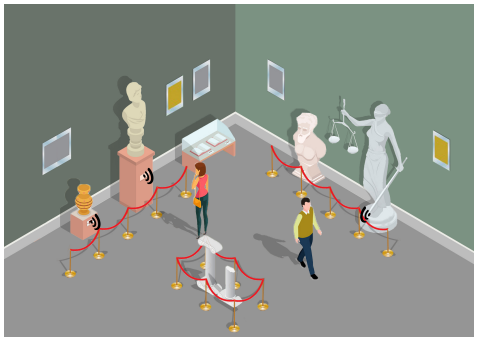

Fig. 1. Sketch of a tracking scenario inside a museum. Device-free visitors move spontaneously around the exhibits which are RFID-tagged.

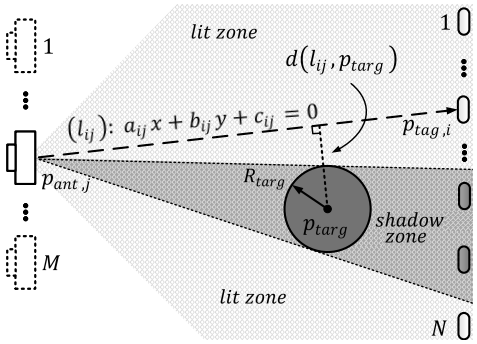

Fig. 2. A circular target divides the reading zone of the antenna to the lit and shadow sub-zones. A Line-of-Sight (LOS) link is preserved for the tags of the lit zone.

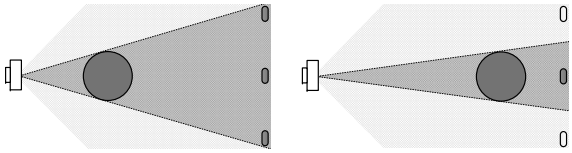

Fig. 3. The distance between the target and the antenna determines the size of the shadow zone and thus, the number of the obscured links. A rough estimation can be intuitively obtained even by a single antenna.

target with respect to time. Eventually, a Savitzky–Golay filter [16] is deployed for further smoothing the estimated trajectory.

In contrast to prior art, this method exploits the phase of the backscattered signal, since RSS is more sensitive to multipath and properties of the propagation environment. It was found that disturbances in the phase patterns capture more efficiently the signal's interference by the target movement. Furthermore, this work realises the target as a cylinder. Instead of a point mass, a target that holds a cylindrical volume inside the space facilitates the development of more effective geometrical-based models. Under such perspective, single-antenna schemes can be employed; when more tags are obscured, the cylindrical target should reside closer to the antenna, as indicated in Fig. 3. On the contrary, localization methods utilizing a point mass model, require inefficient and expensive deployment of multiple antennas around the search space.

Being independent of any training or fingerprinting data sets, the method does not require excessive offline preparation. The only prerequisite is the recording of the radio profiles in a target-free environment, a process that can be easily implemented at no expense of time or effort; e.g. such measurements can be collected periodically overnight.

This work is part of a larger project which aims to track visitors inside the Archaeological Museum of Thessaloniki, see Fig.1. The objectives are among others the extraction of visiting patterns and collection of various statistical data regarding the visitors' behavior. The latter do not necessarily carry any RFID-enabled device, while the exhibits inside the museum areas are RFID-tagged and interrogated by the antennas mounted in one side of the room.

II. Solution Approach

A. Geometrical Configuration

Consider the geometry of Fig. 2, where M antennas are monitoring a group of N tags. Let $\boldsymbol{p}_{ant,j} = (x_{ant,j}, y_{ant,j})$ and $\boldsymbol{p}_{tag,i} = (x_{tag,i}, y_{tag,i})$ denote the known coordinates of the j^{th} antenna and the i^{th} tag, respectively. The LOS link between them is denoted as l_{ij} and it can be geometrically intercepted as a line $(l_{ij}) : a_{ij}x + b_{ij}y + c_{ij} = 0$, where $a_{ij} = y_{tag,i} - y_{ant,j}$, $b_{ij} = -x_{tag,i} + x_{ant,j}$ and $c_{ij} = -y_{tag,i}x_{ant,j} + y_{ant,j}x_{tag,i}$.

The presence of a human inside the monitored area is expected to influence the propagation environment by interfering with some of the links. Instead of a point mass, the target holds a circular volume of radius R_{targ} and center $\boldsymbol{p}_{targ} = (x_{targ}, y_{targ})$, as depicted in Fig. 2. The reading zone of each antenna is divided into two sub-zones, the lit and the shadow, the boundaries of which are nominally determined by the tangent lines from the antenna-point to the circular target surface. The size of the shadowed region and hence, the number of expected obscured links, depends on the distance between the antenna and the target; the closer the target lays to the antenna, the wider the shadow zone becomes. This effect is depicted in Fig. 3, which indicates that target localization is feasible in two dimensions even by a single antenna.

Let $d\left(l_{ij}, \boldsymbol{p}_{targ}\right)$ denote the perpendicular distance between the target's centroid and the link-line l_{ij} :

$$d\left(l_{ij}, \boldsymbol{p}_{targ}\right) = \frac{|a_{ij}x_{targ} + b_{ij}y_{targ} + c_{ij}|}{\sqrt{a_{ij}^2 + b_{ij}^2}} \tag{1}$$

According to the above geometrical relationship, links with distance (1) shorter than the target's radius are nominally obscured by the target, whereas those with greater distance are not. The expected obstruction-state of the link can be then defined such that a value of 1 indicates blocking and a value of 0 not. The state depends on the target location and thus, its binary form is given by:

$$e_{ij}(\boldsymbol{p}_{targ}) = \begin{cases} 1, & if\ d\left(l_{ij}, \boldsymbol{p}_{targ}\right) \leq R_{targ} \\ 0, & otherwise \end{cases} \tag{2}$$

Eventually, the expected states of all links are stacked into an $N \times M$ matrix $\boldsymbol{E}(\boldsymbol{p}_{targ})$. Assuming a grid of hypothetical

Authorized licensed use limited to: Aristotle University of Thessaloniki. Downloaded on September 26,2022 at 08:46:46 UTC from IEEE Xplore. Restrictions apply.

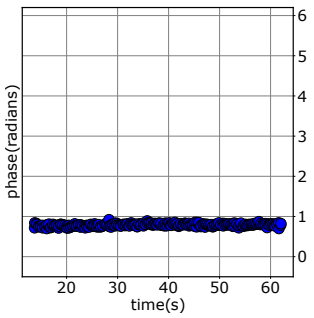

Fig. 4. A typical phase profile measured in a target-free environment. Phase is Gaussian distributed and therefore exhibits small random variations with standard deviation less than 0.1rads.

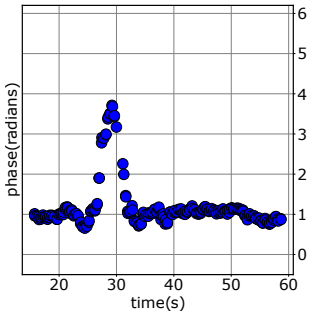

Fig. 5. A phase profile disturbed by a target crossing the antenna-to-tag line of sight. Apart from small random noise, the profile exhibits time-dependent fluctuations due to the target movement.

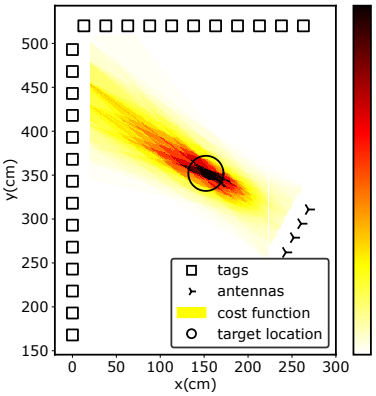

Fig. 6. Representation of similarity function (4) computed for a grid of possible target locations. High amplitudes are depicted by hotter colors. The maximum values of (4) are recorded in the vicinity of the actual target location depicted by a circle.

target locations over the search-space, the expectation link state matrix for each of them can be computed and stored during an offline phase.

B. Target-free Environment

In an offline phase, each antenna records the phase of each tag's signal for a long-time in the environment devoid of target. Phase has support in $[0, 2\pi]$, therefore phase unwrapping is deployed to eliminate 2π jumps and drops that may mislead the algorithm. In an empty propagation environment, the unwrapped phase profiles do not exhibit any significant variation over time. Fig. 4 shows a characteristic phase curve. Phase obeys a typical Gaussian distribution with a standard deviation of less than 0.1 radians. Being time-independent, such profiles can be sufficiently represented by statistical values. Contextually, for the unwrapped phase profile of the i^{th} tag measured by the j^{th} antenna, the average value $\overline{\mathbf{\Phi}}^0_{ij}$ and read rate ρ^0_{ij} are computed and stored for further usage.

C. Target Occurrence

As the human target moves inside the propagation environment, the shadow zone of each antenna changes and different antenna-to-tag LOS links are obscured. However, even if a tag falls in the shadow zone, the power of the diffraction field is likely to be adequate to activate it. Fig. 5 plots a typical measured phase-profile when a target moves in the vicinity of the tag. In contrast to the phase of Fig. 4 obtained in a target-free environment, this profile exhibits disturbances depending on the target's movement over time.

Let t denote the time and estimation index. Since the tags are not replying to the reader simultaneously, the estimation is based on measurements collected within a short-time window that corresponds to index t. The window has a length of δ and should be long enough to acquire measurements from all antenna-tag pairs. However, at the same time, it should not be too long. Otherwise, a rapid target movement will not be detected. The measurements within a short-time window exhibit no significant variation and they too, can be represented by the average unwrapped phase $\overline{\mathbf{\Phi}}^t_{ij}$ and read rate ρ^t_{ij}. The differences between them and the target-free average values recorded in the offline phase are evaluated to determine the measured binary state of each link. More specifically:

$$m^t_{ij} = \begin{cases} 1, if \left(\Delta\overline{\mathbf{\Phi}}^t_{ij} \geq \gamma_\phi\right) or \left(\Delta\rho^t_{ij} \leq \gamma_\rho\right) \\ 0, otherwise \end{cases} \tag{3}$$

where $\Delta\overline{\mathbf{\Phi}}^t_{ij} = |\overline{\mathbf{\Phi}}^t_{ij} - \overline{\mathbf{\Phi}}^0_{ij}|$, $\Delta\rho^t_{ij} = \rho^t_{ij}/\rho^0_{ij}$ and γ_ϕ, γ_ρ are predefined thresholds. The read-rate evaluation essentially identifies cases of full blocking where no measurements of a tag are collected within the considered time window. Eventually, the $N \times M$ matrix $\boldsymbol{M}^t$ stacks the states m^t_{ij} of all links.

The (dis)similarity between matrices $\boldsymbol{M}^t$ and $\boldsymbol{E}(\boldsymbol{p}_{targ})$ represents the probability of the assumed target location $\boldsymbol{p}_{targ}$ to be the actual one at timestep t. This resemblance should be quantified such that its magnitude is directly proportional to the number of true positives - i.e. links with expected and measured state same and equal to one, $m^t_{ij} = e_{ij} = 1$ - and inversely proportional to the amount of false positives and false negatives - i.e. links with unequal states $m^t_{ij} \neq e_{ij}$.

$$g(\boldsymbol{M}^t, \boldsymbol{E}\left(\boldsymbol{p}_{targ}\right)) = \frac{\sum_{j=1}^{M}\sum_{i=1}^{N} m^t_{ij} e_{ij}}{\sum_{j=1}^{M}\sum_{i=1}^{N} |m^t_{ij} - e_{ij}|} \tag{4}$$

The nominator corresponds to the algebraic representation of an AND logical operation outputting 1 when both of its inputs are equal to 1. The denominator represents an XOR operation which outputs 1 only for unequal inputs. Fig. 6 illustrates the magnitude of (4) based on actual measurements for a grid of possible target locations. High amplitudes are depicted by hot colors, while white and black color correspond to zero and maximum cost-values, respectively.

D. Tracking of a Moving Target

Tracking a moving target refers to the estimation of its dynamic state with respect to time. Let the state vector at time instant t consist of the target's location and velocity along each axis of motion, namely $\boldsymbol{X^t} = [x^t, y^t, u^t_x, u^t_y]^T$. The tracking

Authorized licensed use limited to: Aristotle University of Thessaloniki. Downloaded on September 26,2022 at 08:46:46 UTC from IEEE Xplore. Restrictions apply.

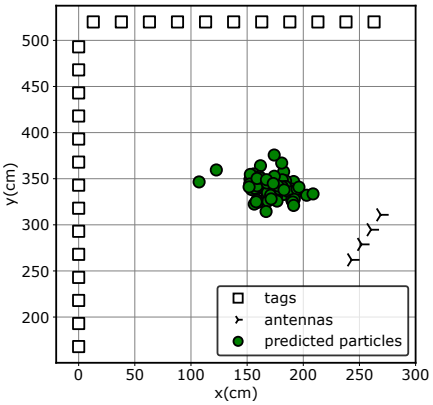

Fig. 7. Predict step:
The temporal evolution of the particle states is performed according to the transition model (6) and the previous state.

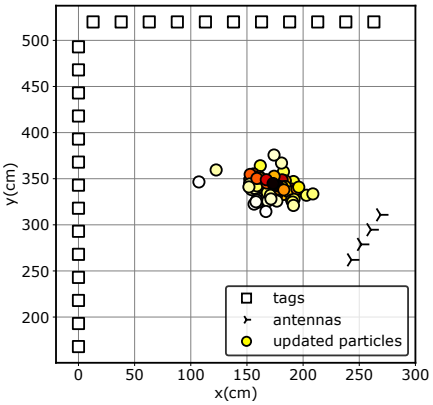

Fig. 8. Update step: The particle weights are chromatically represented. Hotter colors correspond to highly-weighted particles, whereas white represents zero weights.

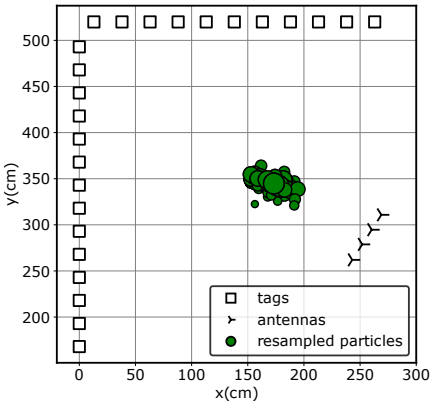

Fig. 9. Resampling step: The size of each particle represents the times it has been drawn. The larger the depiction of a particle, the more copies have been generated from it.

process can be discriminated in two main operations: i) prediction and ii) update. Prediction is related to the temporal evolution of the target state depending on previous states, while update stage refers to the modification of the predicted state in the light of new measurements.

Particle filters (PF) solve the estimation problem by employing a set of weighted particles, each of which represents a potential state accompanied by its likelihood to be the actual one:

$$\{\boldsymbol{X}_n^t, w_n^t\}_{n=1}^{N_p} \tag{5}$$

where w_n^t is the importance weight of the n^{th} particle and N_p the particle population. The implemented PF algorithm consists of the following steps:

1) Initialization: Initially, a swarm of N_p particles is randomly generated within the search space boundaries, while all weights are set to $1/N_p$.

2) Prediction: Prediction corresponds to the temporal evolution of each particle's state based on the previous state and a transition model. Assuming a short duration Δt between the successive time instants $t-1$ and t, the maneuvers of a human target in Δt are expected to be random and can be efficiently intercepted by a white noise acceleration model. According to the latter, the acceleration of the target $\boldsymbol{a}_n^t = [a_{x_n}^t, a_{y_n}^t]^T$ along each motion axis is an independent Gaussian process with standard deviation σ_a for each of its components. In matrix form, the state of each particle is predicted according to:

$$\boldsymbol{X}_n^t = \boldsymbol{F}\boldsymbol{X}_n^{t-1} + \boldsymbol{B}\boldsymbol{a}_n^t, \quad n \in [1, N_p] \tag{6}$$

where $\boldsymbol{F} = \begin{bmatrix} 1 & 0 & \Delta t & 0 \\ 0 & 1 & 0 & \Delta t \\ 0 & 0 & 1 & 0 \\ 0 & 0 & 0 & 1 \end{bmatrix}$, $\boldsymbol{B} = \begin{bmatrix} \Delta t^2/2 & 0 \\ 0 & \Delta t^2/2 \\ \Delta t & 0 \\ 0 & \Delta t \end{bmatrix}$.

The predicted states of the particles are presented in Fig. 7.

3) Update: The update step attempts to modify the weights by incorporating measurements. The similarity function $g\left(\boldsymbol{M}^t, \boldsymbol{E}\left(\boldsymbol{X}_n^t\right)\right)$ given by (4), quantifies the likelihood of the n^{th} particle to be the true one. Therefore, each weight is updated according to

$$w_n^t = w_n^{t-1} g\left(\boldsymbol{M}^t, \boldsymbol{E}\left(\boldsymbol{X}_n^t\right)\right), \quad n \in [1, N_p] \tag{7}$$

At last, the updated weights are normalised such that:

$$w_n^t = \frac{w_n^t}{\sum_1^{N_p} w_n^t}, \quad n \in [1, N_p] \tag{8}$$

The updated weights of the particles are depicted in Fig. 8.

4) Estimation: The weighted mean of the particles' states represents the estimation of the target's location at time instant t:

$$\overline{\boldsymbol{X}}^t = \sum_{n=1}^{N_p} w_n^t \boldsymbol{X}_n^t \tag{9}$$

5) Resampling: A danger concealed in particle filters is the particle degeneracy, namely the case where all particle weights with the exception of one eventually tend to zero. In order to tackle this issue, a resampling step is included. N_p particles are selected from the existed set of particles, while their probability to be drawn is proportional to their weights. As a consequence, the improbable small-weighted particles are discarded and replaced with copies of highly-weighted particles. Fig. 9 shows this procedure, where the size of each particle represents the amount of times it has been copied.

After the resampling phase the algorithm returns to the step of prediction and the procedure is repeated at each time step t, until the target exits the monitored area.

6) Smoothing: Eventually, a polynomial-based filter [16] is applied to smoothen the estimated trajectory.

III. Experimental Evaluation

The experiments were conducted inside a multipath-rich laboratory area. 25 passive UHF RFID tags were placed at $1m$ height forming a Γ-like shape across the room, with an inter-tag spacing of $25cm$. In the opposite side of the space, four patch antennas connected to the same reader were employed at a similar height with an inter-antenna spacing of only $20cm$,

Authorized licensed use limited to: Aristotle University of Thessaloniki. Downloaded on September 26,2022 at 08:46:46 UTC from IEEE Xplore. Restrictions apply.

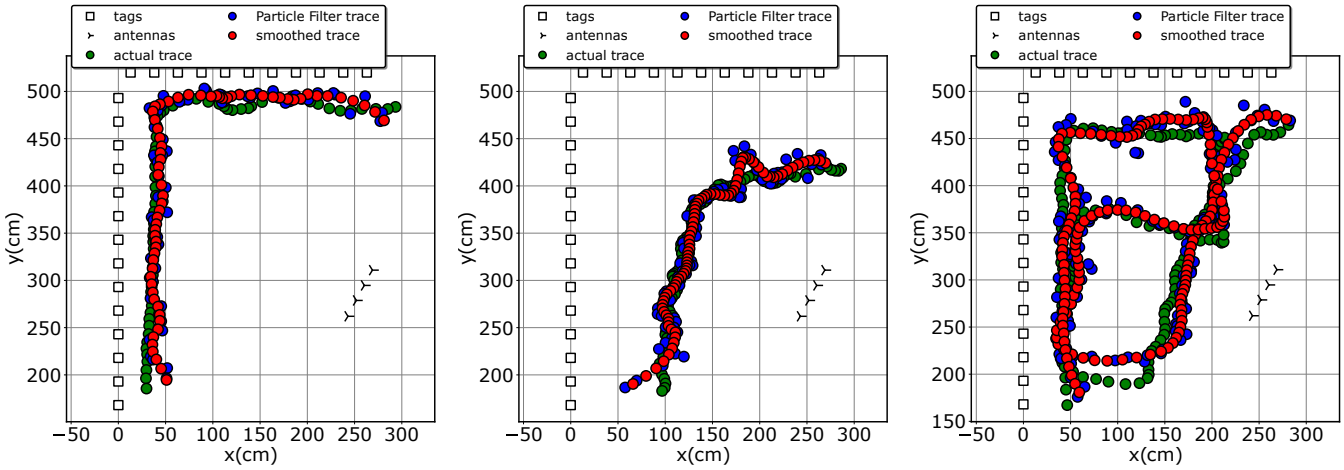

Fig. 10. The target paths for three of the experiments where the target moved across Γ-like and arbitrary paths. Green color depicts the trajectory derived by the camera-based system, blue color represents the path estimated by the PF algorithm and red color corresponds to the eventual trajectory after the deployment of the smoothing filter.

Fig. 11. Photo of the experimental set-up, where 4 antennas were employed opposite to 25 passive tags. The human target moves across the enclosed space carrying an ArUco marker such that the ground truth of its trace is measured.

as shown in Fig. 11. During the experiments, a single human target is travelling at various speeds and trajectories through the enclosed space, which corresponds to a search volume of $3.5m \times 2.5m$.

The static locations of the antennas and tags, as well as the human's trajectory, were measured by employing AruCo markers; i.e. paper-printed markers composed by inner black and white squares, the sequence of which determines a specific ID. A camera-enabled laptop continuously monitors the area and the acquired images are evaluated to detect and identify markers. Then, the position and rotation of the identified markers with respect to the camera is estimated. During the experiments, the human carries an ArUco marker and the above vision-based system tracks its locations. These are used as ground truth and compared to locations estimated by the proposed DFL method.

Experiments took place in two phases. During the offline phase, measurements were taken in a target-free space and the average phase value and read rate of each antenna-to-tag pair were recorded. Furthermore, benefited from the facts that the tags and antennas locations do not change and the expected link state depends only on the hypothetical target location, the expected state matrices for all possible positions within the search-space, were computed in advance and stored. In such manner, these calculations no longer need to be made in the online phase and the computational cost of the algorithm is relaxed.

The online phase refers to the evaluation of the proposed method. During this step, a single human target moves spontaneously across the space. An estimation is derived every $\Delta t = 0.5s$. The length of the measurement time-window is set to $\delta = 0.5s$, the standard deviation of the acceleration $\sigma_a = 0.5m/s^2$, the thresholds $\gamma_\phi = 1rad$ and $\gamma_\rho = 0.25$ and the particle population $N_p = 200$. Regarding the latter, increasing the number of particles not only did not improve the achieved accuracy but also increased needlessly the computational burden.

A. Experimental Results

Fig. 10 depicts the estimated trajectories for three of the experiments by utilizing all available links composed by the 4 antennas and the 25 tags.

1) Effect of the target radius: Fig. 12 explores the achieved accuracy for different radii of the target. Lowest localization error is achieved when a target radius of $20cm$ or $25cm$ are considered, reporting a median accuracy of $18cm$.

2) Effect of the target speed: Fig. 13 examines the impact of the target's speed on the performance for a radius of $25cm$. In particular, an experiment of Γ-like path was repeated for three different walking speeds labeled as slow, medium and fast. The method preserves its robustness for all speeds, reporting equivalent accuracy with a median error around $15cm$, while no error greater than $35cm$ was observed.

3) Effect of the number of antennas: Next, the performance of the method is investigated with respect to the number of employed antennas. Fig. 14 indicates the localization error slightly decreases with the increase of the antennas. When a

Authorized licensed use limited to: Aristotle University of Thessaloniki. Downloaded on September 26,2022 at 08:46:46 UTC from IEEE Xplore. Restrictions apply.

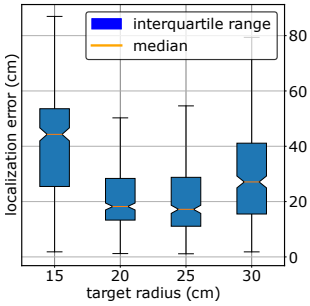

Fig. 12. Localization error for varying the radius of the target. The median, maximum, minimum and interquartile range are presented.

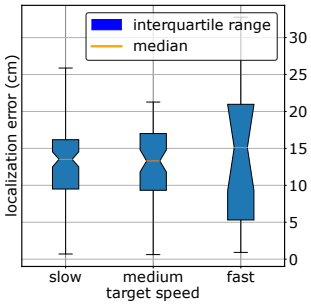

Fig. 13. Localization error for varying the experimental speed of the target. The median, maximum, minimum and interquartile range are presented.

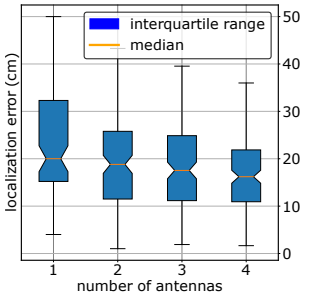

Fig. 14. Localization error for varying the number of employed antennas.The median, maximum, minimum and interquartile range are presented.

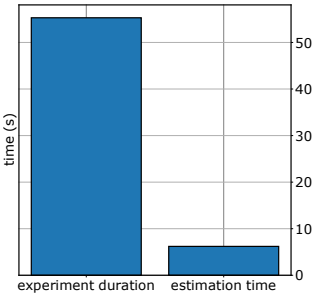

Fig. 15. Average time required to estimate the target's trajectory, compared to the average duration of the experiment.

single antenna is utilized, a median error of $20cm$ is achieved, which decreases to about $15cm$ when all four available antennas are taking into account. The accomplished accuracy is adequate for realistic applications making the method suitable even for single-antenna schemes.

4) Estimation-time: The only time-consuming operation of the method is the calculation of expected link states $\boldsymbol{E}(\boldsymbol{X}_n^t)$ for each employed particle. However, by including this process in the offline stage and store the values in the memory, the computational complexity is reduced. Fig. 15 verifies the real-time capability of the method, which requires around $40ms$ to make a single estimation.

IV. Conclusion

This work presents a device-free tracking scheme, that tracks a single human target by exploiting a network of passive RFID tags inside the monitored area. As the target moves through the environment, it blocks some antenna-to-tag links and influences their phase measurements. By comparing them with measurements collected from a target-free environment in a prior offline phase, the binary state of the link can be determined; i.e. whether the link is affected or not. Information about each link-state is then mapped to the target's location by employing a geometrical model, according to which the target holds a cylindrical volume. Thanks to such assumption, target localization can be achieved even when a single antenna is available. A particle filter algorithm is developed to constantly update the target's location over time. Experimental results report a median error of slightly less than $20cm$, while the computational cost of the algorithm is negligible.

References

[1] Y. Guo, K. Huang, N. Jiang, X. Guo, Y. Li and G. Wang, "An Exponential-Rayleigh Model for RSS-Based Device-Free Localization and Tracking," in IEEE Transactions on Mobile Computing, vol. 14, no. 3, pp. 484-494, 1 March 2015, doi: 10.1109/TMC.2014.2329007.

[2] O. Kaltiokallio, M. Bocca and N. Patwari, "A Fade Level-Based Spatial Model for Radio Tomographic Imaging," in IEEE Transactions on Mobile Computing, vol. 13, no. 6, pp. 1159-1172, June 2014, doi: 10.1109/TMC.2013.158.

[3] Z. Wang, H. Liu, S. Xu, X. Bu and J. An, "A Diffraction Measurement Model and Particle Filter Tracking Method for RSS-Based DFL," in IEEE Journal on Selected Areas in Communications, vol. 33, no. 11, pp. 2391-2403, Nov. 2015, doi: 10.1109/JSAC.2015.2430517.

[4] B. Mager, P. Lundrigan and N. Patwari, "Fingerprint-Based Device-Free Localization Performance in Changing Environments," in IEEE Journal on Selected Areas in Communications, vol. 33, no. 11, pp. 2429-2438, Nov. 2015, doi: 10.1109/JSAC.2015.2430515.

[5] C. Xu, B. Firner, Y. Zhang, R. Howard, J. Li and X. Lin, "Improving RF-based device-free passive localization in cluttered indoor environments through probabilistic classification methods," 2012 ACM/IEEE 11th International Conference on Information Processing in Sensor Networks (IPSN), 2012, pp. 209-220, doi: 10.1109/IPSN.2012.6920958.

[6] J. Wang, X. Zhang, Q. Gao, H. Yue and H. Wang, "Device-Free Wireless Localization and Activity Recognition: A Deep Learning Approach," in IEEE Transactions on Vehicular Technology, vol. 66, no. 7, pp. 6258-6267, July 2017, doi: 10.1109/TVT.2016.2635161.

[7] B. Wagner, D. Timmermann, G. Ruscher and T. Kirste, "Device-free user localization utilizing artificial neural networks and passive RFID," 2012 Ubiquitous Positioning, Indoor Navigation, and Location Based Service (UPINLBS), 2012, pp. 1-7, doi: 10.1109/UPINLBS.2012.6409762.

[8] Zhang J, Xiao W, Zhang S, Huang S. Device-Free Localization via an Extreme Learning Machine with Parameterized Geometrical Feature Extraction. Sensors. 2017; 17(4):879. https://doi.org/10.3390/s17040879

[9] D. Zhang, Y. Liu, X. Guo and L. M. Ni, "RASS: A Real-Time, Accurate, and Scalable System for Tracking Transceiver-Free Objects," in IEEE Transactions on Parallel and Distributed Systems, vol. 24, no. 5, pp. 996-1008, May 2013, doi: 10.1109/TPDS.2012.134.

[10] Y. Zhao, N. Patwari, J. M. Phillips and S. Venkatasubramanian, "Radio tomographic imaging and tracking of stationary and moving people via kernel distance," 2013 ACM/IEEE International Conference on Information Processing in Sensor Networks (IPSN), 2013, pp. 229-240, doi: 10.1145/2461381.2461410.

[11] B. Wagner, N. Patwari and D. Timmermann, "Passive RFID tomographic imaging for device-free user localization," 2012 9th Workshop on Positioning, Navigation and Communication, 2012, pp. 120-125, doi: 10.1109/WPNC.2012.6268750.

[12] Y. Ma, B. Wang, X. Gao and W. Ning, "The Gray Analysis and Machine Learning for Device-Free Multitarget Localization in Passive UHF RFID Environments," in IEEE Transactions on Industrial Informatics, vol. 16, no. 2, pp. 802-813, Feb. 2020, doi: 10.1109/TII.2019.2921529.

[13] J. Wang, J. Xiong, H. Jiang, X. Chen and D. Fang, "D-Watch: Embracing "Bad" Multipaths for Device-Free Localization With COTS RFID Devices," in IEEE/ACM Transactions on Networking, vol. 25, no. 6, pp. 3559-3572, Dec. 2017, doi: 10.1109/TNET.2017.2747583.

[14] J. Han et al., "Twins: Device-Free Object Tracking Using Passive Tags," in IEEE/ACM Transactions on Networking, vol. 24, no. 3, pp. 1605-1617, June 2016, doi: 10.1109/TNET.2015.2429657.

[15] M. Ghaddar, L. Talbi, T. A. Denidni and A. Sebak, "A Conducting Cylinder for Modeling Human Body Presence in Indoor Propagation Channel," in IEEE Transactions on Antennas and Propagation, vol. 55, no. 11, pp. 3099-3103, Nov. 2007, doi: 10.1109/TAP.2007.908563.

[16] A. Savitzky, M.J.E. Golay, "Smoothing and Differentiation of Data by Simplified Least Squares Procedures", Analytical Chemistry, 36 (8): 1627–39,1964

Authorized licensed use limited to: Aristotle University of Thessaloniki. Downloaded on September 26,2022 at 08:46:46 UTC from IEEE Xplore. Restrictions apply.